Energy Conversion and Management 162 (2018) 241–255

Contents lists available at ScienceDirect

Energy Conversion and Management

journal homepage: www.elsevier.com/locate/enconman

The characterization of dynamic behavior of Li-ion battery packs for enhanced design and states identification

Woochul Nam[a], Ji-Young Kim[b], Ki-Yong Oh[c,*]

[a] School of Mechanical Engineering, Chung-Ang University, 84 Heukseok-ro, Dongjak-gu, Seoul 06974, Republic of Korea
[b] Renewable Energy Group, Korea Electric Power Corporation Research Institute, Munjiro 105, Daejeon 34056, Republic of Korea
[c] School of Energy System Engineering, Chung-Ang University, 84 Heukseok-ro, Dongjak-gu, Seoul 06974, Republic of Korea

ARTICLE INFO

Keywords:
Diagnosis
Evolution of elastic modulus
Lithium-ion battery pack
Li-ion intercalation
Sensor placement

The dynamic responses of a Li-ion battery pack deployed on hybrid electric vehicles are studied with a high fidelity finite element model and a parametric reduced-order model. The effects of microstructure transformation in the electrode materials caused by lithium-ion intercalation/deintercalation on the evolution of dynamic responses are investigated including the effects of the state of charge, aging, and cell-to-cell variations. The dynamic responses obtained from a finite element analysis show two interesting phenomena. First, the high modal density is controllable with the design modification of a pack component. Second, dynamic responses, especially the evolution of the natural frequencies of the fixed-boundary modes, of a Li-ion battery pack provide useful information to estimate the dynamic states or health states of the battery. A probabilistic analysis is also carried out considering stochastic operational conditions of hybrid electric vehicles with a parametric reduced-order model. The probabilistic analysis not only suggests appropriate modes and locations for monitoring its dynamic responses, but also determines the maximum response level of every cell in the battery pack. The proposed modeling approach can improve the safety and reliability of the structural design of battery cells and packs. Furthermore, it can be useful for the identification of the battery states during the operation.

1. Introduction

Li-ion Batteries (LIBs) are free from several deficiencies that occur in other secondary cells, such as high self-discharge rates [1] and memory effect [2]. LIBs also have a higher energy economy than other secondary batteries [3]. These advantages enable LIBs to dominate the portable electronics market and establish them as promising reversible power sources for electric powered vehicles [4].

The lifespan and aging [5] of LIBs are major concerns that limit their application in the electric transportation markets. To ensure the lifespan of LIBs during operation, significant efforts have been devoted to two research areas. The first area is focused on optimization of the design of battery cells and packs. The second area is focused on development of enhanced control methodologies embedded in the battery management system.

Mechanical stresses from Li-ion intercalation and temperature variation should be considered in the design of LIBs. Dynamic and accumulated stresses affect performance and degradation of LIBs [6].

Several studies on mechanical characteristics of LIBs have been conducted. Anode swelling was measured and correlated with microscopic lattice expansion of graphite to elucidate the swelling mechanism [7]. An image processing technique used optical images to observe reversible strains during lithiation of a graphite electrode [8]. Neutron radiography was addressed to quantify the lithium concentration over the state of charge (SOC) [9]. Strain-induced stress of a graphite anode was characterized with a micro-Raman mapping technique [10]. Changes in the mechanical properties of separators over life cycles have been investigated to determine their relationship with degradation in cell performance and capacity loss with simulations [11] and experiments [12]. Stress evolution in a silicon thin-film electrode was measured by using a multi-bean optical sensor technique [13]. A modal test was conducted to measure frequency responses of a single pouch cell over the SOC [14].

Thermal issues have been studied because the lifespan and states of LIBs are affected by temperature [15]. Advanced thermal management apparatuses were suggested to control operational temperature. These apparatuses include a liquid metal [16], a cold plate [17], a heat pipe [18], phase change materials [19], and composite phase change materials [20]. Thermal optimization was conducted for a LIB pack under extreme operational conditions [21]. Thermal abuse was simulated to

* Corresponding author.
E-mail address: kiyongoh@cau.ac.kr (K.-Y. Oh).

https://doi.org/10.1016/j.enconman.2018.02.022

Available online 21 February 2018

Nomenclature

E_{neg}	modulus of elasticity of the negative electrode, GPa
E_{pos}	modulus of elasticity of the positive electrode, GPa
$i\delta_{SOC}$	uniform internal of SOC
k_{eq}	equivalent stiffness, Nm^{-1}
k_i	stiffness of the ith layer, Nm^{-1}
P_{neg}	porosity of the negative electrode
P_{pos}	porosity of the positive electrode
ΔSOC	interval of the SOC
SOC_0	fully discharged state
x_{Li}	Li concentration in the anode
$\mathbf{K}_i$	Stiffness matrix at several SOC, Nm^{-1}
$\mathbf{K}_i^{FEM}$	stiffness matrix of the full-order model of the component i, Nm^{-1}
$\mathbf{K}_i^{PROM}$	reduced-order stiffness matrix of the component i, Nm^{-1}
$\mathbf{K}_0^{PROM}$	reduced-order stiffness matrix at the fully discharged state, Nm^{-1}

elucidate effects of high temperature on capacity degradation [22]. Novel thermal management strategies [23] such as a lattice Boltzmann method [24] were also suggested. These studies generally used a 3-D finite element analysis to elucidate thermal behaviors of LIBs [24].

Multiple studies have been conducted to improve performance of battery management systems. These efforts can be classified into three categories: modeling, states estimation, and power management.

A variety of models, including a first order model with an integrator [25], a 1-D electrochemical model [26], an empirical dynamic voltage model [27], and a support vector machine based model [28] were proposed. An enhanced single particle model was suggested to consider temperature dependency when estimating the SOC [29]. A lumped thermal dynamic model [30], a coupled electro-thermal model [31], and a phenomenological multi-physics model [32] were also suggested for use in thermal management. A dynamic modeling procedure for real-time control of a LIB pack was proposed [33]. Performance and accuracy of these models were recently compared for application in electric vehicles (EVs) [34].

A Kalman filter [35], an adaptive Kalman filter [36], and a generic algorithm [37] were proposed with open-circuit voltage [38] and dynamic impedances [39] to estimate the SOC. Several methods including a neural network [40], an adaptive neuro-fuzzy [41], and an indirect non-intrusive method [42] were suggested with a single-point impedance [43] and on-board internal resistance estimation [44] to estimate the state of health (SOH). Recently, the error sources of online state estimation methods were investigated using error flow charts [45].

Several algorithms have been suggested for advanced power management. These efforts include an adaptive load compensator [46], demand response programming [47], convex programming [48], a Bayesian predictive modeling technique [49], efficiency maps [50], a hybrid approach [51], a cost-emission model [52], an equivalent consumption minimization strategy [53], a sliding model controller [54], and a sensorless quick charger [55]. Convex relaxations in the optimal control [56] and integrated optimization of battery sizing, charging, and power management [57] were also studied. A method for enhanced sample entropy-based health management was proposed for EVs [15].

Several studies addressed mechanical responses for characterizing dynamic states at the cell level [58]. Several phenomenological models have been proposed to predict the strain [59] and stress [60] of a cell. A modified stress model was suggested based on strain measurements by using a real-time optical acquisition system [61]. A coupled electro-chemical, thermal, and mechanical model of LIBs was also suggested and validated with experiments [62]. These studies offer potential viability of mechanical measurements to develop a new generation of state estimation [63], health management [64], and power management [65] of battery management systems for EVs and hybrid electric vehicles (HEVs). However, Li-ion intercalation and phase transition [66] have not been considered in-depth in the pack level despite the fact that the periodic stresses caused by Li-ion intercalation and phase transition affect performance and degrade cells during operation.

To overcome these limitations, this study characterizes the dynamic responses and their evolution on the pack level for the first time with a high fidelity finite element model (FEM) and a parametric reduced-order model (PROM). The proposed modeling methods enable one to predict dynamic responses of a LIB pack and their evolution in a variety of deterministic and stochastic conditions. Specifically, the effects of evolution of mechanical properties of the electrodes on changes in dynamic responses are investigated. Studying dynamic responses and their evolution using a high fidelity model is difficult because of computational complexity. Heavy computational effort impedes a probabilistic analysis on the dynamic responses even though the fatigue life strongly depends on their vibration response. Deterministic analyses

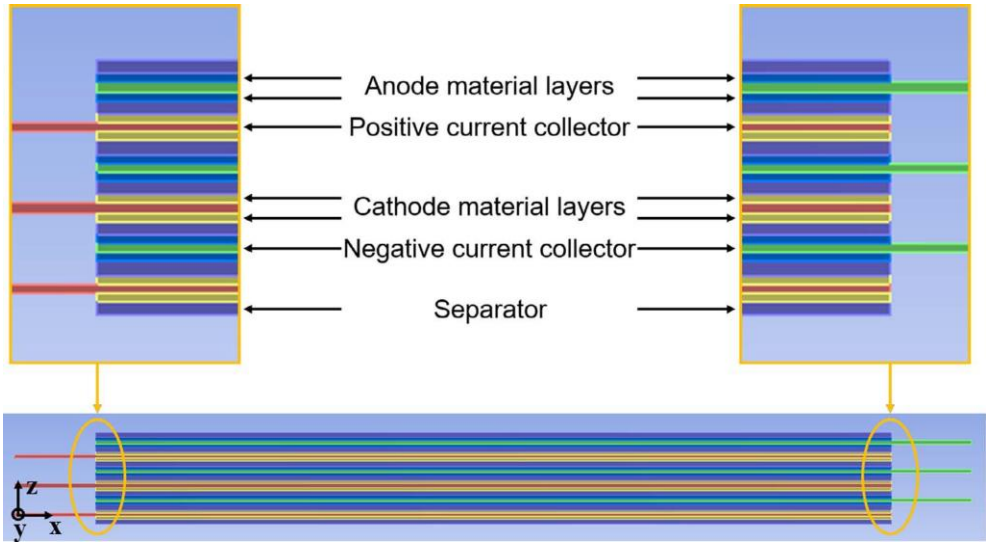

Fig. 1. Geometry of the jellyroll used in this study: the orange and green domains represent positive and negative current collectors, respectively. The yellow and blue domains represent the cathode and anode material layers coated on both sides of the current collector, respectively. The purple domain represents the separators located between the positive and the negative electrodes.

with the FEM characterized two interesting features of LIBs in both design and state identification. First, it was revealed that the high modal density, which is a significant concern on a battery pack, was manageable with modification to the pack design. Second, dynamic responses at the fixed-boundary modes were more sensitive than at other modes, suggesting that this information is useful for state identification of the pack. Stochastic analyses with the PROM provided useful results over a variety of operational conditions for EVs. These results include appropriate modes to detect faults and cell aging, the maximum response level for every cell, and optimal locations to place sensors for monitoring the LIB pack. These results are an important contribution of this study because the effects of microstructure transformation in electrodes on the SOC and SOH of the pack are significant.

2. Modeling methods

This section discuss modeling methods for a high fidelity 3-D FEM and a PROM proposed in this study. Section 2.1 describes 3-D FEM of a pack and material properties used in simulation. Section 2.2 introduces a method to construct the PROM from its mother FEM.

2.1. 3-D finite element model

A prismatic LIB cell, deployed on EVs or HEVs, is modeled replicating the battery cell used in a Ford Fusion HEV. The prismatic Li-ion cell is used widely in EVs and HEVs because it has a better stacking efficiency and higher volumetric density when assembled in a pack [67]. Fig. 1 shows the geometry of the jellyroll modeled in this study. This jellyroll is placed inside the aluminum casing of the battery cell. The dimensions of the jellyroll were modeled with the information obtained from the dissection with the length of 110 mm (x direction in Fig. 1), the height of 75 mm (y direction in Fig. 1), and the width of 11.4 mm (z direction in Fig. 1).

Three sandwich-structures are stacked in series in the z direction. Each sandwich consists of an aluminum positive current collector coated on both sides with the lithium manganese oxide material ($Li_xMn_2O_4$), a microporous polyethylene separator material, and a copper negative current collector coated on both sides with a graphite intercalation material (Li_xC_6) [68]. The thicknesses (z direction in Fig. 1) of each current collector, active material, and separator are 400 μm, 400 μm, 600 μm, respectively. The length (along the x direction) of current collectors is slightly larger than that of the active materials and the separators because the left and right sides (x direction in Fig. 1) of the current collectors are connected to the positive and negative terminals. It is possible to model a cell as small numbers of thick sandwiches instead of large numbers of thin sandwiches to reduce the heavy computational efforts. The equivalent stiffness of a cell is the same for both cases if total thickness of each component is the same in a cell. Note that the equivalent stiffness k_{eq} of springs in series can be obtained as $1/k_{eq} = \Sigma\ 1/k_i$, where is k_i the stiffness of the ith layer.

Thus, three sandwiches with relatively larger thickness are used to identify the overall dynamic characteristics of a LIB pack. In a previous study [69], it is proposed that a pack consisting of three cases, three jellyrolls, and three spacers can be represented as four spring components; three jellyrolls are represented as two spring elements in parallels to account for their nonlinearity. Previous studies have addressed similar approaches not only to identify the dynamic responses [60] and thermal responses [22] of battery cells and packs, but also to reduce the heavy computational effort of a full-order model.

The simplified academic model of an LIB pack consists of 20 nominally identical cells stacked in the battery pack (Fig. 2). Plastic spacers are modeled replicating the spacer of a Ford fusion HEV battery pack [65]. Then, they are placed between the battery cells and at the ends of the pack to preserve the airflow channels for cooling. These spacers also maintain the compression between cells.

The dynamic model is focused on a small deformation because a large deformation only occurs due to external forces, such as a crash. However, this external force is unlikely to be applied to the battery system under the normal operation conditions. Under this small deformation, the slip motion (along shear direction) is relatively very small. Therefore, this slip motion is not considered in contacting surfaces in the system: interfaces between the components in the jellyroll, interfaces between the case and the jelly roll, and interfaces between the spacer and the case of the cell.

A Hex-dominant meshing method was used in the structural analysis package in ANSYS to generate the mesh of the model. This method was used to generate hexahedral meshes for the jellyroll because of its simple geometry. In contrast, tetrahedral elements were created for the case and the spacer because these components had more complex shapes than the jellyroll. The degrees of freedom (DOF) for the proposed pack model is the order of 10^6. This model is sufficient to characterize the dynamic characteristics of the LIB pack because it reflects the basic topology and the key characteristics of the pack.

This model mainly incorporates the evolution in the modulus of elasticity over the SOC and the SOH to estimate the effect of these variations on the dynamic responses of a LIB pack. The variation in the modulus of elasticity over the SOC is caused by material transformation [66]. The variation over the SOH is caused by the stiffening of the anode (due to aging) and by the formation of solid electrolyte inter- phase [70]. The changes in the modulus of elasticity of the anode, which is coated on both sides of the negative current collector, over the SOC is estimated as

$$E_{neg}(x_{Li}) = (19.25 + 82.23x_{Li})\cdot(1 - 1.9P_{neg} + 0.9P_{neg}^2), \quad (1)$$

where E_{neg} is the modulus of elasticity of the anode, x_{Li} is the Li concentration in the negative electrode, and P_{neg} is the porosity of the negative electrode. The modulus of elasticity of the anode is linearly dependent on the Li concentration [71]. The correction factor was introduced to take into account the effect of the porosity of the anode [72] because the anode is a porous structure to percolate the electrolyte through the pores and allow the transport mechanisms of the lithium ion [74]. In this study, the value that reflects the porosity of the anode P_{neg} is determined as 0.444 [75]. The porosity of the negative electrode P_{neg} is ranged from 0.357 to 0.485 from literatures [76–84], suggesting that the used porosity of the negative electrodes P_{neg} is reasonable because the used porosity is around the middle of ranges.

Similarly, the modulus of elasticity of the positive electrode E_{pos} is obtained taking into consideration a correction factor that reflects its porosity as

$$E_{pos} = 25\cdot(1 - 1.9P_{pos} + 0.9P_{pos}^2), \quad (2)$$

where the porosity of the positive electrode P_{pos} is 0.357 [75]. The porosity of the lithium manganese oxide material ($Li_xMn_2O_4$) measured

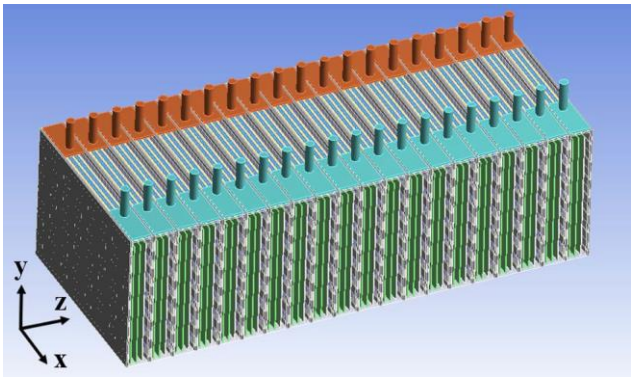

Fig. 2. Geometry of the LIB pack model. The orange and sky blue domains represent positive and negative terminals, respectively. The gray domain represents spacers between the battery cells. The green domain represents negative current collectors on the side of the cells (the aluminum cases of the cells are not pictured).

by X-ray microscopy is 0.363 and 0.380 depending on equipment [85], suggesting that the porosity of the positive electrode P_{pos} applied is reasonable. The modulus of elasticity for the cathode is assumed to be constant over the SOC. The volume change of the cathode is below 1%. Thus, it is plausible to assume that the change in this material property is negligible [73].

The changes in the estimated modulus of elasticity over the SOC for the anode and the cathode are shown in Fig. 3. As the SOC increases, Li-ions move from the cathode to the anode and the modulus of elasticity of the anode is increased by the change that takes place in its microstructure due to the Li-ion intercalation. The modulus of elasticity for the separator and aluminum were determined as 437 MPa and 68 GPa, respectively [86]. The Poisson's ratios for the active materials and the separator are determined as constant values (i.e., 0.24 and 0.3, respectively) because the Poisson's ratio does not significantly change with the Li concentration [71].

The mode shapes and dynamic responses of the battery pack are calculated using ANSYS. All material properties except those of the negative electrode are considered independent of the Li-ion concentration and temperature. The nodes on the left end of the pack are fixed in the modal analysis.

Three possible cases of variations in the modulus of elasticity under different operational conditions are considered to identify the dynamic characteristics of a battery pack. First, the effects of the SOC on the dynamic responses of the battery pack are analyzed. This case identifies the changes in the dynamics of the battery packs (represented by the changes in the modulus of elasticity (Fig. 3)) when they are charged/discharged under normal operational conditions. Second, the evolution of the modulus of elasticity caused by degradation is analyzed to elucidate the evolution of dynamic responses due to aging of the battery pack. This case incorporated the stiffening effect on the modulus of elasticity. Third, the effects of the structural variations on the dynamic responses are analyzed. It is important to investigate the effects of variations among the cells because those variations can lead to stress localization, which results in concentrating the vibration energy in one or more cells that in turn leads to an increase of the forced response. This case incorporated the variation in the modulus of elasticity of several cells. In addition, statistical dynamic responses are calculated to account for the effects of cell-to-cell variations with thousands of different variations.

2.2. Parametric reduced-order model

The level of the maximum forced response of cells in a battery pack is a key metric to evaluate its safety and reliability. Intensive vibrations and stress concentration on a single cell can lead to local degradation and failure of the entire pack. To evaluate the maximum forced response for every cell in a battery pack, thousands of different cell-to-cell variations should be simulated for a probabilistic analysis considering the stochastic operational conditions. This analysis could be performed by using the Monte Carlo simulations. However, this method is computationally expensive because it has to consider several possible cases using a FEM of a battery pack with significant degree of freedom (DOF). For example, the FEM of the simplified academic battery pack has 1,344,438 DOF. The computational time to perform Monte Carlo simulations with the FEM would be considerably long. This study introduced a PROM [87], which can account for the cell-to-cell variation, to avoid the expensive process of conducting several analyses. Modes of interest are selected to describe its dominant dynamics when the PROM is constructed. Thus, the PROM can accurately predict the dynamic responses which are almost same with results of the full-order FEM model with much lower computational cost.

The key idea of the PROM is the parameterization of the stiffness matrices. Any variation in the range of interest can be applied without several analyses of the full-order FEM. Hong et al. proposed the PROM, which can account for the structural variation in the cells and predict the dynamic responses caused by prestress [87]. This work modified the previous PROM and applied it to larger and more complex LIB packs to obtain more realistic results. Note that the previous PROM based work [87] assumed the battery cell as a single metal plate. Hence, the work was not able to consider the microstructure transformation in electrode materials and complex geometry. The method proposed in [87] is modified to accurately predict the dynamic responses over the SOC. This improvement enables one to study the structural cell-to-cell variations for identification of the dynamic characteristics of the packs.

This study proposes that changes in stiffness can be calculated with the fifth-order polynomial equation of the SOC. Based on this idea, the stiffness matrices can be constructed as

$$\mathbf{K}(SOC_0 + \Delta SOC) \approx \mathbf{K}_0 + (\Delta SOC)\mathbf{K}_1 + (\Delta SOC)^2\mathbf{K}_2 + (\Delta SOC)^3\mathbf{K}_3 + (\Delta SOC)^4\mathbf{K}_4 + (\Delta SOC)^5\mathbf{K}_5, \quad (3)$$

where $\mathbf{K}_i$ (for i = 0–5) is the stiffness matrix at several SOC, SOC_0 is the fully discharged state, i.e. 0% SOC, and ΔSOC is the interval of the SOC. Six equations are needed to calculate the matrices $\mathbf{K}_i$. To calculate these six equations, the reduced-order stiffness matrix $\mathbf{K}_i^{PROM}$ is computed for six parameter values as

$$\mathbf{K}^{PROM} = (\mathbf{T}^{PROM})^T \mathbf{K}^{FEM} \mathbf{T}^{PROM}, \quad (4)$$

where $\mathbf{T}^{PROM}$ and $\mathbf{K}_i^{FEM}$ are the transformation matrix and the stiffness matrix of the full-order model of the component i, respectively [88]. In the fully discharged state, the stiffness matrix can be expressed as

$$\mathbf{K}(SOC_0) \approx \mathbf{K}_0^{PROM}, \quad (5)$$

Then substituting ΔSOC into $i\delta_{SOC}$ (with i = 1, 2, 3, 4, 5) where $i\delta_{SOC}$ is the uniform interval of 0.2 results in

$$\mathbf{K}(SOC_0 + i\delta_{SOC}) \approx \mathbf{K}_i^{PROM} \approx \mathbf{K}_0 + (i\delta_{SOC})\mathbf{K}_1 + (i\delta_{SOC})^2\mathbf{K}_2 + (i\delta_{SOC})^3\mathbf{K}_3 + (i\delta_{SOC})^4\mathbf{K}_4 + (i\delta_{SOC})^5\mathbf{K}_5, \quad (6)$$

Rearranging Eqs. (5) and (6) into a matrix form leads to

$$\mathbf{C}\begin{bmatrix}\mathbf{K}_{0,eq}\\ \mathbf{K}_{1,eq}\\ \mathbf{K}_{2,eq}\\ \mathbf{K}_{3,eq}\\ \mathbf{K}_{4,eq}\\ \mathbf{K}_{5,eq}\end{bmatrix} = \begin{bmatrix}\mathbf{K}(SOC_0)_{eq}\\ \mathbf{K}(SOC_0 + \delta_{SOC})_{eq}\\ \mathbf{K}(SOC_0 + 2\delta_{SOC})_{eq}\\ \mathbf{K}(SOC_0 + 3\delta_{SOC})_{eq}\\ \mathbf{K}(SOC_0 + 4\delta_{SOC})_{eq}\\ \mathbf{K}(SOC_0 + 5\delta_{SOC})_{eq}\end{bmatrix}, \quad (7)$$

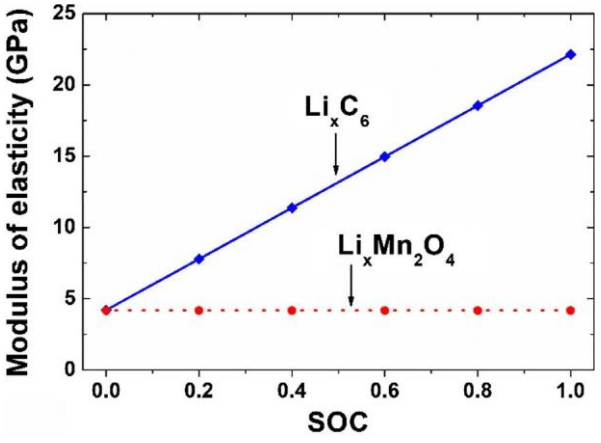

Fig. 3. Evolution of modulus of elasticity with the SOC in the positive and negative electrodes.

where $\mathbf{C} = \begin{bmatrix} 1 & 0 & 0 & 0 & 0 & 0 \\ 1 & \delta_{SOC} & (\delta_{SOC})^2 & (\delta_{SOC})^3 & (\delta_{SOC})^4 & (\delta_{SOC})^5 \\ 1 & 2\delta_{SOC} & (2\delta_{SOC})^2 & (2\delta_{SOC})^3 & (2\delta_{SOC})^4 & (2\delta_{SOC})^5 \\ 1 & 3\delta_{SOC} & (3\delta_{SOC})^2 & (3\delta_{SOC})^3 & (3\delta_{SOC})^4 & (3\delta_{SOC})^5 \\ 1 & 4\delta_{SOC} & (4\delta_{SOC})^2 & (4\delta_{SOC})^3 & (4\delta_{SOC})^4 & (4\delta_{SOC})^5 \\ 1 & 5\delta_{SOC} & (5\delta_{SOC})^2 & (5\delta_{SOC})^3 & (5\delta_{SOC})^4 & (5\delta_{SOC})^5 \end{bmatrix}$. Eq. (7) is solved using the inverting the 6 × 6 matrix C. The inverse matrix A is defined as

$$\mathbf{A} = \mathbf{C}^{-1} = \begin{bmatrix} A_{11} & A_{12} & A_{13} & A_{14} & A_{15} & A_{16} \\ A_{21} & A_{22} & A_{23} & A_{24} & A_{25} & A_{26} \\ A_{31} & A_{32} & A_{33} & A_{34} & A_{35} & A_{36} \\ A_{41} & A_{42} & A_{43} & A_{44} & A_{45} & A_{46} \\ A_{51} & A_{52} & A_{53} & A_{54} & A_{55} & A_{56} \\ A_{61} & A_{62} & A_{63} & A_{64} & A_{65} & A_{66} \end{bmatrix}. \quad (8)$$

Rearranging Eq. (5) using the entries of A, one obtains

$$\begin{aligned} \mathbf{K}(SOC_0 + \Delta SOC) &\approx \mathbf{K}^{PROM}_{\Delta SOC} \\ &\approx b_0\mathbf{K}^{PROM} + b_1\mathbf{K}^{PROM} + b_2\mathbf{K}^{PROM} + b_3\mathbf{K}^{PROM} \\ &\quad + b_4\mathbf{K}^{PROM} + b_5\mathbf{K}^{PROM}, \end{aligned} \quad (9)$$

where

$$b_0 = A_{11} + A_{21}\Delta SOC + A_{31}(\Delta SOC)^2 + A_{41}(\Delta SOC)^3 + A_{51}(\Delta SOC)^4, + A_{61}(\Delta SOC)^5$$

$$b_1 = A_{12} + A_{22}\Delta SOC + A_{32}(\Delta SOC)^2 + A_{42}(\Delta SOC)^3 + A_{52}(\Delta SOC)^4 + A_{62}(\Delta SOC)^5,$$

$$b_2 = A_{13} + A_{23}\Delta SOC + A_{33}(\Delta SOC)^2 + A_{43}(\Delta SOC)^3 + A_{53}(\Delta SOC)^4 + A_{63}(\Delta SOC)^5,$$

$$b_3 = A_{14} + A_{24}\Delta SOC + A_{34}(\Delta SOC)^2 + A_{44}(\Delta SOC)^3 + A_{54}(\Delta SOC)^4 + A_{64}(\Delta SOC)^5,$$

$$b_4 = A_{15} + A_{25}\Delta SOC + A_{35}(\Delta SOC)^2 + A_{45}(\Delta SOC)^3 + A_{55}(\Delta SOC)^4 + A_{65}(\Delta SOC)^5,$$

$$b_5 = A_{16} + A_{26}\Delta SOC + A_{36}(\Delta SOC)^2 + A_{46}(\Delta SOC)^3 + A_{56}(\Delta SOC)^4 + A_{66}(\Delta SOC)^5.$$

The parameterized stiffness matrix in Eq. (9) is used to estimate the structural dynamic responses of the battery pack with different levels of the SOC.

3. Results and discussion

This section examines simulation results and discussion. Section 3.1 describes deterministic responses from 3-D FEM simulations. Section 3.2 describes probabilistic responses from the Monte Carlo simulations with the PROM.

3.1. Deterministic responses

The natural frequencies of the simplified academic battery pack corresponding to the mode index at the fully discharged state (0.0 SOC) are shown in Fig. 4 (a). The battery pack features a high modal density at a mode index higher than 70, which is similar to the result provided from the previous study [87]. The high modal density means that the natural frequencies in a mode cluster are close to each other. This phenomenon take place in periodic structures mounted on a stiff frame in general. High modal density is critical to the fatigue lifetime of systems because random structural variations might concentrate the vibration energy on a narrow local area if the excitation contains frequencies in the region of high modal density. This characteristic is known as the Anderson localization [89]. Local stress concentration is also harmful to a battery pack because local stress concentration results in local degradation in several cells which decreases the overall performance of the battery pack.

The mode shapes are analyzed to identify the dynamic characteristics of the pack. The difference in the mode shape between the previous study [87] and this study is caused by the different geometries of the two battery packs. First, the high modal density caused by the terminals is not predicted in [87] because the terminals are not modeled. However, our results suggest that a short circuit or disconnection can occur in terminals due to the concentration of the vibration energy. Hence, more attention should be paid to the design of the terminals to mitigate the problems of high modal density in the motion of terminals. Second, in contrast to the previous study, the high modal density due to a fixed-boundary mode is not obtained in this study. The spacers considered in this study had many dimples. Because these spacers undermine the fixed-boundary motions, high modal density is not predicted in this study. This observation suggests that an appropriate design of the spacers could mitigate problems caused by high modal density, which can result in the concentration of vibration energy on local area. These results imply that the modal analysis provides much valuable information to optimize the design of a battery pack.

The changes in the natural frequency for different SOC with respect to 0.0 SOC are plotted in Fig. 4(b). The red dashed-dotted-dotted line, the blue dashed line, the orange dotted line, the green dashed-dotted line, and the purple line denote the shift in the natural frequencies at 0.2 SOC, 0.4 SOC, 0.6 SOC, 0.8 SOC, and 1.0 SOC (with respect to 0.0 SOC), respectively. The shifts in the natural frequency of each mode increase with charging because the equivalent modulus of elasticity of batteries in a pack increases over the SOC due to Li-ion intercalation in the negative electrodes.

As shown in Fig. 4(b), the levels of shifts in the natural frequency for the mode indexes less than 60 are considerably higher than those for the mode indexes larger than 60. As aforementioned, the modes from index 61 to 100, which are hereafter called the terminal modes, are mainly originated from the motion of the positive and negative terminals (orange[1] and light green domains in Fig. 2). The effect of material transformation in the jellyroll on the terminal modes is very small.

Periodic picks are observed in the shifts of natural frequencies from 0.0 SOC to the higher values of SOC (Fig. 4(b)). To elucidate the nature of these periodic picks, six modes corresponding to the picks are analyzed (Fig. 5). The figure shows that all mode shapes resulting in significant shifts in the natural frequency are the mode shapes of a fixed-boundary cell, which are hereafter called the swelling modes. The first swelling mode shapes (12th, 18th, and 27th modes) are shown in the top of Fig. 5, and the second swelling mode shapes (17th, 25th, and 35th modes) are shown in the bottom of Fig. 5. These swelling modes are sensitive to Li-ion intercalation because the evolution of modulus of elasticity over the SOC in the negative electrode results in changes in the equivalent stiffness of the jellyroll. Therefore, the swelling modes of the cells show significant shifts compared to the other modes. It is expected that this phenomenon would be more significant in the actual battery pack in the sense that the jellyroll is clamped and welded to the buss bars at the edge sides to secure the positions of the jellyroll in the prismatic cells [68]. These components create additional constraints and increase the equivalent stiffness in the edges of the cells, and consequently grow the magnitude of the fixed-boundary modes in a battery pack.

Fig. 6 shows the shifts (in percentage) of each mode with respect to the frequency of each mode at 0.0 SOC. The red circle markers, the blue diamond markers, and the hexagon markers represent the first (1st), second (2nd), and third (3rd) swelling modes, respectively. The swelling shapes of the third swelling modes are similar to those of the

[1] For interpretation of color in Fig. 2, the reader is referred to the web version of this article.